universe MDPI

Article

Collisional Broadening within a Hadronic Transport Approach

Branislav Balinovic [1,2], Renan Hirayama [2,3,*] and Hannah Elfner [1,2,3,4]

[1] Institut für Theoretische Physik, Goethe Universität, Max-von-Laue-Strasse 1, 60438 Frankfurt am Main, Germany; balinovic@fias.uni-frankfurt.de (B.B.); elfner@itp.uni-frankfurt.de (H.E.)
[2] Frankfurt Institute for Advanced Studies, Ruth-Moufang-Strasse 1, 60438 Frankfurt am Main, Germany
[3] Helmholtz Forschungsakademie Hessen für FAIR (HFHF), GSI Helmholtzzentrum für Schwerionenforschung, Campus Frankfurt, Max-von-Laue-Str. 12, 60438 Frankfurt am Main, Germany
[4] GSI Helmholtzzentrum für Schwerionenforschung, Planckstr. 1, 64291 Darmstadt, Germany
* Correspondence: hirayama@fias.uni-frankfurt.de; Tel.: +49-69-798-47678

Abstract: We explore the emergence of the collisional broadening of hadrons under the influence of different media using the hadronic transport approach SMASH (Simulating Many Accelerated Strongly interacting Hadrons), which employs vacuum properties and contains no a priori information about in-medium effects. In this context, we define collisional broadening as a decrease in the lifetime of hadrons, and it arises from an interplay between the cross-sections for inelastic processes and the available phase space. We quantify this effect for various hadron species, in both a thermal gas in equilibrium and in nuclear collisions. Furthermore, we distinguish the individual contribution of each process and verify the medium response to different vacuum assumptions; we see that the decay width that depends on the resonance mass leads to a larger broadening than a mass-independent scenario.

Keywords: hadronic transport; resonance properties; collisional broadening

check for updates

Citation: Balinovic, B.; Hirayama, R.; Elfner, H. Collisional Broadening within a Hadronic Transport Approach. *Universe* **2023**, *9*, 414. https://doi.org/10.3390/universe9090414

Academic Editors: Péter Kovács, Sándor Lökös and Dániel Kincses

Received: 17 July 2023
Revised: 23 August 2023
Accepted: 1 September 2023
Published: 9 September 2023

1. Introduction

The properties of Quantum Chromodynamics (QCD) at finite temperature and finite baryochemical potential are not well understood, as they comprise a region of the phase diagram difficult to access both in experiments and in first-principle theories. In the confined phase, the degrees of freedom consist of colorless hadrons, and the system evolution is well described by hadronic transport. As a baseline for any further medium modifications, it is of interest to understand how hadron properties are modified when embedded in a hadronic medium.

One natural change caused by the presence of a medium is the reduction in hadron lifetimes due to absorption processes. The usual prescription in hadronic transport approaches is to associate the lifetime (τ^{vac}) of a resonance in vacuum with the inverse of its width, such that its decay in a small time interval $\Delta\tau$ happens as a Bernoulli trial with probability $P_{\text{decay}}(\Delta\tau) = \Gamma^{\text{vac}}\Delta\tau$. Here, Γ^{vac} is called *vacuum decay width*, and the medium-induced shortening of lifetimes can be thought of as an effective increase in the width. This effect is known as *collisional broadening*.

From a historical and experimental perspective, medium modifications are studied by comparing elementary collisions and heavy-ion collisions (HICs), scaling the observable appropriately. Specifically, the NA60 Collaboration revealed that the softening of the invariant mass spectra of dileptons [1] around the ρ meson pole mass is consistent with the in-medium broadening of vector mesons proposed by Rapp et al. [2,3]. This was later covered in off-shell hadronic transport approaches—where the hadron spectral function can change dynamically during propagation—by including a collisional width explicitly parameterized as a linear function of the local density [4,5]. On the other hand, on-shell hadronic transport approaches use the coarse-graining method: the average of several collisions gives local values for thermodynamic quantities, with which the corresponding rates from the in-medium model are computed [6–8].

In [8], dilepton emission was included and found to be in agreement with experimental yields in elementary collisions at HADES energies but not in the heavy-ion yields around the ρ meson pole mass, showing that the collisional broadening intrinsic to hadronic transport is not sufficient to account for the full effect of a medium. In [9], we studied the collisional broadening of ρ in an equilibrated hadron gas and in nuclear collisions. The thermal gas exhibited a spectral function similar to the full in-medium model but expectedly less broadened.

In this work, we extend that previous study to some resonances of particular interest, determine the processes that contribute the most to ρ collisional broadening, and investigate the effect of the two different model assumptions usually chosen for the vacuum properties of resonances in hadronic transport. This paper is organized as follows: Section 2 describes the aspects of the SMASH approach relevant to this work. In Sections 3.1 and 3.2, we display the behavior of the dynamically generated collisional broadening of different particles in a thermal scenario and in nuclear collisions, respectively. In Section 3.3, we compare the collisional broadening of ρ and ω mesons under different vacuum assumptions. A brief summary of the results is given in Section 4, along with a discussion of their interpretation. Appendix A shows the inelastic cross-sections of some relevant interactions.

2. SMASH Transport Approach

In this study, we used the hadronic transport approach SMASH-2.2 (Simulating Many Accelerated Strongly interacting Hadrons) to simulate different states of nuclear matter, such as a thermal gas in equilibrium and nuclear collisions [10]. In this microscopic transport approach, the complete information of the phase space is accessible at all times according to effective solutions of the relativistic Boltzmann equation.

We employ the geometric collision criterion of SMASH to determine possible scatterings, in which an interaction can happen if

$$d_{\text{trans}} < d_{\text{int}} = \sqrt{\frac{\sigma_{\text{tot}}}{\pi}}\,, \tag{1}$$

where σ_{tot} is the total cross-section and d_{trans} is the distance between two particles in a given time interval in the center of the mass frame. With this criterion, the only possible processes are binary: resonance formation ($2 \to 1$), its corresponding resonance decay ($1 \to 2$), as well as elastic and inelastic scatterings ($2 \to 2$). To account for multi-particle interactions, intermediate resonances are produced or decay in a chain. The available species, their vacuum mass M_0 and pole width Γ_0, possible decay channels, and associated branching ratios are taken from Particle Data Group 2016 [11].

The mass of a new resonance is constant during propagation and randomly chosen at production using the normalized vacuum spectral function

$$\mathcal{A}^{\text{vac}}(m) = \frac{2\mathcal{N}}{\pi}\frac{m^2\Gamma^{\text{dec}}(m)}{(m^2 - M_0^2)^2 + [m\Gamma^{\text{dec}}(m)]^2} \tag{2}$$

as a probability distribution, where normalization factor $\mathcal{N}$ is defined by the relation

$$1 = \int_{m_{\text{min}}}^{\infty} \mathcal{A}^{\text{vac}}(m)\, dm, \tag{3}$$

with threshold mass m_{min} being equal to the sum of masses from its lightest decay channel. The *mass-dependent* decay width is based on the Manley formalism [12], given by

$$\Gamma^{\text{dec}}_{R\to ab}(m) = \Gamma^0_{R\to ab}\frac{\rho_{ab}(m)}{\rho_{ab}(M_0)}, \tag{4}$$

where $\Gamma^0_{R\to ab}$ is the partial width at the pole mass and $\rho_{ab}(\sqrt{s})$ is a mass-dependent function evaluating the available phase space for the creation of particles a and b from energy $\sqrt{s}$. The total decay width of R in (2) is the sum of the partial widths in (4) over all possible final states ab. If decay happens, the particle decays in a randomly chosen decay channel according to the corresponding branching ratios. Stable hadrons[1] have $\Gamma^{\mathrm{dec}} \approx 0$, so $\mathcal{A}^{\mathrm{vac}}$ reduces to a δ-distribution, and the particle always has pole mass. We also employ a second assumption for vacuum decays to investigate the impact on collisional broadening. Here, $\Gamma^{\mathrm{vac}} = \Gamma_0$ independently of the resonance mass. This is referred to as the *mass-independent* decay assumption.

The SMASH approach uses vacuum properties, so the average lifetime of a particle corresponds to its inverse width only in vacuum. When it is surrounded by other hadrons with which it can interact inelastically, the average lifetime naturally decreases, as illustrated in Figure 1 for a ρ embedded in a medium. We describe this setup in Section 3.1. We notice that the medium suppresses the lifetimes of low-mass particles more, while higher masses are not very affected. This reflects the overall inelastic cross-section between the particle and the rest of the medium.

We remark that this prescription of sampling lifetimes from the (inverse) vacuum width breaks down close to the threshold. The available phase space, ρ_{ab}, approaches 0, so Equation (4) leads to $1/\Gamma^{\mathrm{dec}} \to \infty$, and the resonance can live forever. A more grounded definition was introduced in [13] from the fundaments of quantal scattering theory, associating the lifetime of a resonance with the time delay equal to the derivative of the phase shift, which can be computed analytically from the resonance shape. However, there is no consensus on how to implement this prescription appropriately in real transport model calculations, as it can generate negative time delays or require cross-sections for the "forward-going" part of the resonant wave packet, which are unmeasurable and must be parametrized [14,15]. Therefore, we stick to the usual prescription and investigate the consequences by comparing it to the aforementioned mass-independent assumption, which does not lead to infinite-lasting resonances.

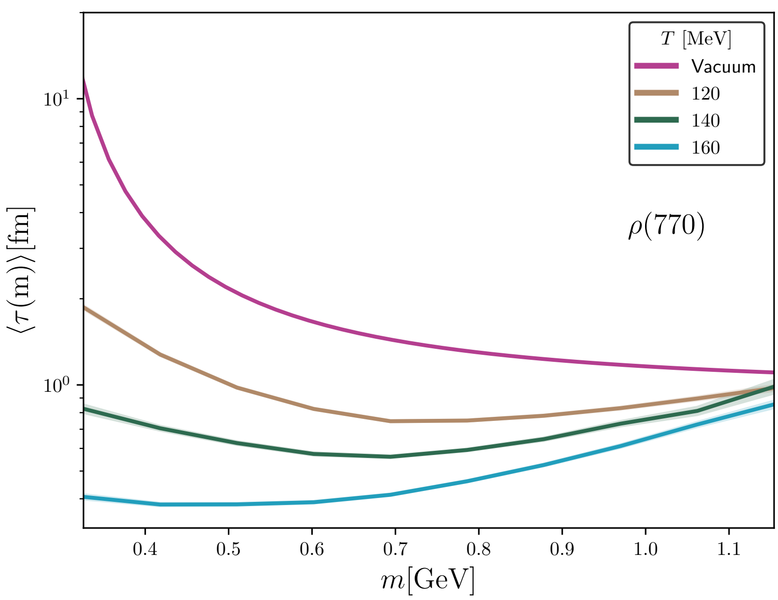

Figure 1. Proper lifetime of the ρ meson for a gas in equilibrium at different temperatures and baryochemical potential $\mu_B = 400$ MeV.

To probe the effect of these inelastic interactions, we follow [9] and define the effective width as

$$\Gamma^{\mathrm{eff}} = \langle\tau\rangle^{-1} = \left\langle \frac{t_f - t_i}{\gamma} \right\rangle^{-1}, \tag{5}$$

where t_i and t_f are the initial time ("birth") and final time ("death") of the particle, respectively, and γ is its Lorentz factor in the computational frame. This definition follows naturally from the prescription we use for the resonance lifetimes in *vacuum*; since they are sampled from the *vacuum* width, the *effective* width should be defined in terms of the *effective* lifetime. In this work, we only consider the dependence of Γ^{eff} on the resonance (on-shell) mass. Because the decays are randomly selected at each time step, it may happen that $\Gamma^{\text{eff}} < \Gamma^{\text{dec}}$ if there is little to no broadening and the statistics are insufficient.

We consider the "death" of a particle when it either decays or scatters inelastically, and we compute γ with its initial momentum. This means that if it goes through elastic scatterings at times $t_1, ..., t_N$ before its death, the exact lifetime is

$$\tilde{\tau} = \frac{t_f - t_N}{\gamma_N} + \frac{t_N - t_{N-1}}{\gamma_{N-1}} + ... + \frac{t_1 - t_i}{\gamma_i}. \tag{6}$$

We checked that this leads to the same effective width as simply computing $\tau = \dfrac{t_f - t_i}{\gamma_i}$ in the analyzed systems. We believe that this happens because the momentum change in elastic collisions is small enough and can be either positive or negative, such that $\langle\tau\rangle \approx \langle\tilde{\tau}\rangle$.

To further quantify collisional broadening, we also define the collisional width as

$$\Gamma^{\text{coll}}(m) = \Gamma^{\text{eff}}(m) - \Gamma^{\text{dec}}(m). \tag{7}$$

Subtracting the contribution of the vacuum from equation (5) results in the contributions solely caused by absorption processes. The medium effects can be further reframed in terms of the *dynamical* spectral function,

$$\mathcal{A}^{\text{dyn}}(m) = \frac{2\tilde{\mathcal{N}}}{\pi} \frac{m^2\Gamma^{\text{eff}}(m)}{(m^2 - M_0^2)^2 + m^2\Gamma^{\text{eff}}(m)^2}, \tag{8}$$

which amounts to replacing the vacuum width in (2) with the effective width (5). Since the system is restricted to finite phase space, the support of this spectral function is not infinite. Therefore, we normalize it with respect to the vacuum spectral function (2):

$$\tilde{\mathcal{N}} = \frac{\int_{m_{\min}}^{m_{\max}} \mathcal{A}^{\text{vac}}(m)dm}{\int_{m_{\min}}^{m_{\max}} \mathcal{A}^{\text{dyn}}(m)dm}, \tag{9}$$

allowing for a proper comparison between the spectral functions for different assumptions. Usually, the expression "spectral function" is used interchangeably with "invariant mass spectra". We find it important to highlight that this is not the case here. The former refers to $\mathcal{A}^{\text{dyn}}$, which encompasses the modifications to the propagator of the resonance, while the latter is denoted by dN/dm and describes the production of resonances; it was also studied in [9,16].

3. Results

3.1. Hadron Gas in Equilibrium

In this section, we demonstrate how particle interactions with a thermal medium affect the effective width (5). To do so, we employ an equilibrated hadron gas with different temperatures T and baryochemical potential $\mu_B = 400$ MeV. The system is simulated with a large box with periodic boundary conditions, initialized with thermal multiplicities according to the given (T, μ_B), and momenta are assigned according to the Boltzmann distribution. To ensure thermalization, we allow the gas to relax and only include particles with $t_i > 1000$ fm, which modifies the nominal (T, μ_B) values. The systems starting at $T = 120/140/160$ MeV fall to $106/128/149$ MeV, respectively. In the following, legends denote the initial temperature, and error bands are statistical.

Since collisional broadening originates from absorption processes, it is also possible to probe it for stable particles. For example, the $\pi\rho \to \omega$ process contributes to the broadening of both π and ρ.

Using (5), we extract the effective width for nucleons and pions. Table 1 shows that similar to ρ, they display an increasing effective width for rising temperatures, and we observe it to be significantly stronger for π than for N. The reason for this is the different number of inelastic channels; many mesonic and baryonic resonances decay into pions, while nucleons only participate in baryonic processes. As the temperature rises, more and more of these channels are opened, so the difference between the effective widths increases.

Table 1. Effective width of stable particles in thermal equilibrium. Errors are statistical.

	Γ^{eff} [GeV]		
T [MeV]	**120**	**140**	**160**
N	0.063 (1)	0.1082 (8)	0.1789 (7)
π	0.0802 (4)	0.2033 (5)	0.4376 (6)

Next, we investigate the collisional broadening of some selected resonances of particular interest. Along with the ρ meson, ω and $\Delta(1232)$ are relevant for dilepton yield, and the latter is also important for pion production, which is famously too high in most transport models. The reconstructability of $K^*(892)$ in HICs was investigated in [17]. $a_1(1260)$ is the chiral partner to ρ, so whether it also broadens is a natural question. Since the average lifetime of the ρ meson is shown in Figure 1, we do not repeat its inverse plot here. The effective width for ω in Figure 2a shows that Γ^{eff} grows with the medium temperature and that the difference from the vacuum is higher at lower masses. The curves converge to the vacuum decay width at large masses, so the decay probability dominates over the absorption probability, meaning that collisional broadening decreases. This happens because the processes that absorb the resonance become less likely, as detailed in Appendix A. We also see a non-monotonic structure in the effective width, caused by the shape of $\Gamma^{\text{dec}}(m)$, which increases relatively sharply while the medium effect decreases.

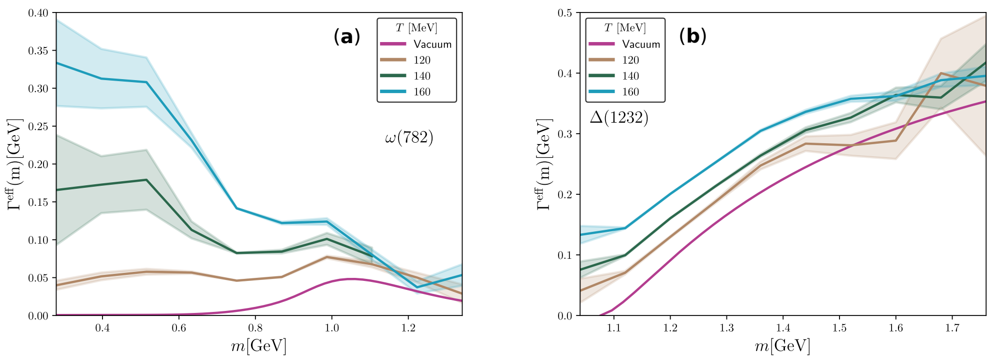

Figure 2. Effective width of (**a**) ω mesons and (**b**) $\Delta(1232)$ baryons in thermal equilibrium.

This convergence at high enough masses is generally shared between the resonances we probe, as shown in Figure 2b for the $\Delta(1232)$ baryon and in Figure 3a for the $K^*(892)$ meson, respectively. Another possible effect coming into play here is that if the vacuum width is large, the particle decays more quickly, so it has less time to scatter inelastically. Unlike the other resonances, low-mass $\Delta(1232)$ do not seem more sensitive to the medium temperature.

Moreover, $a_1(1260)$ does not develop any collisional broadening, as we show in Figure 3b. This is because there is no known process in which it emerges as a decay product; hence, there is no absorption process for it. One possible interesting consequence is that if the a_1 spectral function does broaden in a real QCD medium, as expected if chiral symmetry is restored [2], it has no contribution from collisional broadening, unlike the broadening of the ρ meson, its chiral partner.

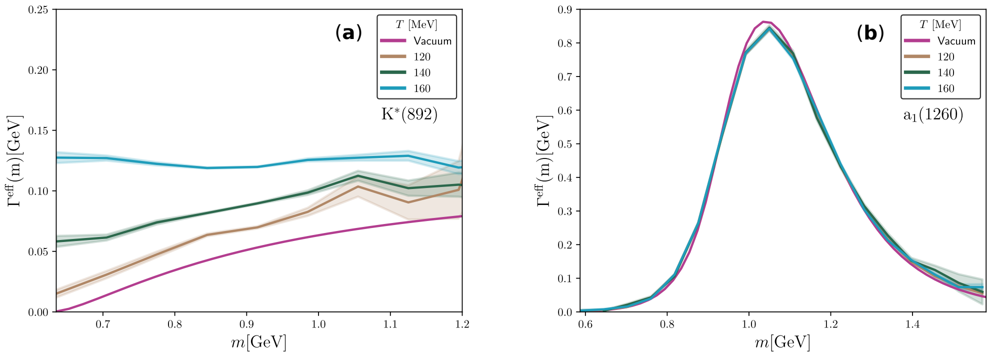

Figure 3. Effective width of (**a**) $K^*(892)$ and (**b**) $a_1(1260)$ mesons in thermal equilibrium.

3.2. Heavy-Ion Collisions

In this chapter, we study the collisional broadening of different particles in the off-equilibrium systems created after HICs. In SMASH, the nucleons in each nucleus are sampled from a Woods–Saxon distribution and move along the z-axis with the input beam energy. One key difference from the thermal hadron gas setup is the presence of strings, representing $2 \to N$ processes. They are formed in an interaction when the incoming particles have sufficient energy and are handled by PYTHIA 8.2 [18]. Another consequence of this initial state is in the system chemistry; in the thermal gas, all possible hadrons are initialized, using the full support of $\mathcal{A}^{\mathrm{vac}}$. On the other hand, HICs start with only nucleons, and the available energy limits the phase space for particle production.

We restrict the analysis to central Au+Au collisions at $1.23A$ GeV kinetic energy and C+C collisions at $1A$ GeV, which are setups run by the HADES experiment at GSI [19,20]. A larger set of systems was investigated in [9], but these two provide a good grasp of the effect of medium size.

Figure 4a shows the effective width of the ω meson, where the broadening increases with system size. Since the vacuum width is small and close to the pole mass, the spectral function (2) is sharp; therefore, particles with masses far from the pole value are rare. For the C+C system, which contains little energy in total, this means that large-mass ω mesons are not produced. Compared with Figure 2a, lower-mass particles have a small broadening. We understand this in light of the medium expansion: as the system expands, the energy available to produce resonances decreases; consequently, lower masses become more likely. At the same time, the medium is diluted; therefore, the broadening of these particles is suppressed.

The $\Delta(1232)$ baryon also broadens more in a collision between heavier nuclei, as we show in Figure 4b. In the C+C collision, lower masses are not produced. The behavior is similar to the thermal gas in Figure 2b, where the collisional broadening displays weak dependence on the mass. This suggests that the Δ baryons behave thermally, with most being created via the first $NN \to N\Delta$ interactions.

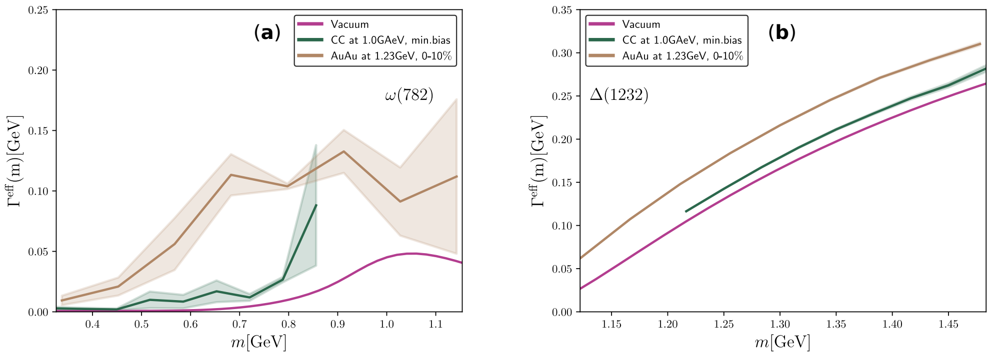

Figure 4. Effective width of the (**a**) $\omega(782)$ meson and (**b**) $\Delta(1232)$ baryon for different nuclear collision systems.

In Figure 5a, we see a small broadening of $K^*(892)$, which increases at high masses in the Au+Au system. In our implementation of low-energy nuclear collisions, the only[2] channel for strange hadron production is the decay of heavier resonances into a strange–antistrange pair. The first NN interactions rarely produce states able to decay into $K^*(892)$ (see Appendix A). Then, at least three interactions must happen to produce it, when the medium may have already become dilute. This is consistent with a previous study that used reconstructable K^* [17]; since they leave the medium before being absorbed, their decay products are also unaffected.

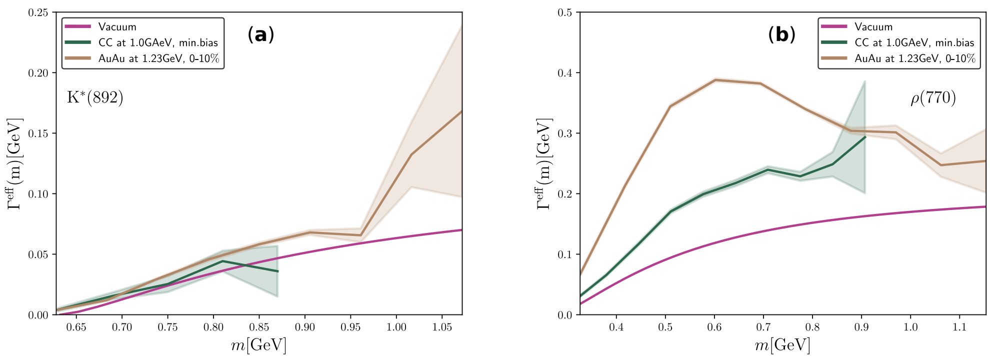

Figure 5. Effective width of the (**a**) $K^*(892)$ and (**b**) ρ mesons for different nuclear collision systems.

Much like in Figure 3b, we do not observe the collisional broadening of the $a_1(1260)$ meson, since there is no process where it is a decay product; therefore, we do not plot the result. We show the effective width of the ρ meson in these collision systems in Figure 5b. Similar to the ω meson, the difference from the thermal gas behavior in lower masses happens because of the medium dilution, since they are mostly produced in the late stage [9].

To discriminate the processes that cause this broadening, we weigh the collisional width (7) with the fraction of each process at a given mass. The dominant contributions are shown in Figure 6 in the Au+Au system. Out of the five most important processes, four are baryonic, similar to the results of Rapp's full in-medium model [2], where ρ couples to nucleons more. As previously suggested in [21], we see a significant contribution from the $\rho N \to N(1520)$ channel around $m \approx 0.5$ GeV. The biggest mesonic contribution is from chiral partner $a_1(1260)$, as was the case in [22] in the same mass range.

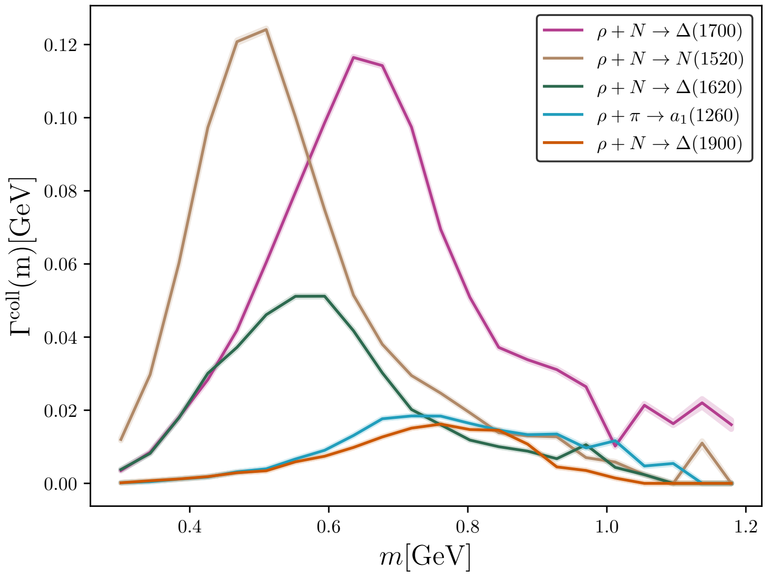

Figure 6. Contributions of the 5 most significant absorption channels to the collisional width of ρ in central Au+Au collisions at 1.23 GeV.

3.3. Collisional Broadening under Different Vacuum Assumptions

In this section, we discuss the effects of the different vacuum decay assumptions (described in Section 2) on collisional broadening. We evaluate the collisional width (7) for both assumptions in the framework of a hadronic thermal gas and show it for ρ and ω in Figure 7, using $\Gamma^0_\rho = 149$ MeV and $\Gamma^0_\omega = 8.5$ MeV. ρ is more broadened in the mass-dependent case, while ω displays a more complicated structure. This arises from different effects:

1. Particles that decay cannot be absorbed, so a larger vacuum width suppresses collisional broadening. At low masses, the vacuum decay width tapers down to 0 in the mass-dependent assumption. This makes the particles more prone to be absorbed by the medium in comparison with the mass-independent case.
2. Inelastic cross-section σ_{ab} affects the broadening of both a and b, since it determines how much one absorbs the other. It has peaks around the pole mass (M^0_R) of possible resonances $ab \to R$ [10]. The masses of the incoming particles control the off-shell mass of the outgoing resonance ($m_R = \sqrt{s_{ab}}$), so such peaks lead to structures in the collisional width of a and b, as exemplified by Figure 6; the contribution of the process $\rho N \to N(1520)$ is higher and close[3] to $M^0_{N(1520)} - m_N = 0.57$ GeV, and heavier resonances lead to peaks in larger m_ρ. This effect is not relevant for very small masses, when $\mathcal{A}^{\mathrm{vac}}_R \to 0$.
3. Absorption cross-section $\sigma_{ab\to R}$ is also proportional to Γ^{vac}_R, so that different mass assumptions give different weights to the resonance peaks.
4. At high enough masses, the absorption cross-section decreases so much that particles stop undergoing collisional broadening, as detailed in Appendix A, such that the vacuum assumption has no effect.

The interplay among the aforementioned effects causes a mass-dependent ρ to always be more absorbed than a mass-independent one. In the case of ω, both cases lead to the same broadening in the range $m_\omega = 0.6 - 0.75$ GeV, but a peak is more pronounced in the mass-dependent assumption in the range $m_\omega = 0.75 - 1.0$ GeV.

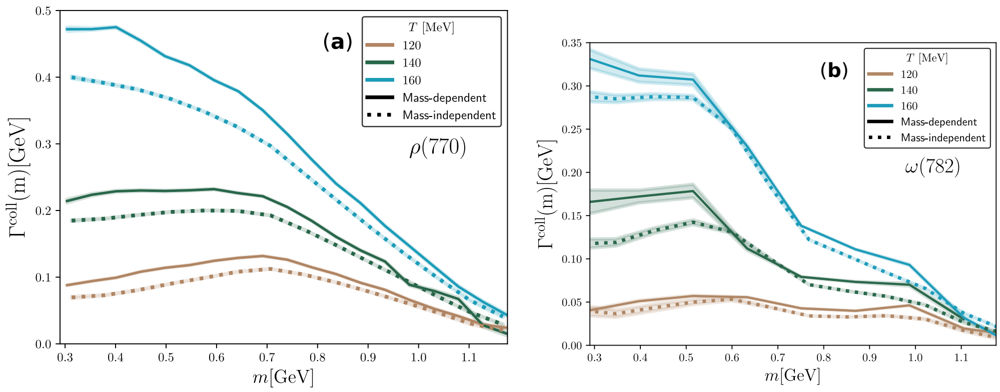

Figure 7. Collisional widths of (**a**) ρ and (**b**) ω in thermal equilibrium under different vacuum decay assumptions.

In order to assess the net effect of both assumptions, we show the corresponding broadened spectral functions ($\mathcal{A}^{\rm dyn}$) in Figure 8, using definition (8) with the same normalization (9) for both assumptions. As expected, the mass-dependent assumption leads to a broader spectral function, but this is only significant around the pole mass.

As mentioned in Section 2, the prescription of setting resonance lifetimes to their inverse widths is not consistent with scattering theory derivations, as they approach infinity close to the threshold. In the mass-independent assumption, this does not happen; subsequently, the medium effect in that region is reduced. In the phase-shift prescription, the time delay (that is, the vacuum lifetime) approaches 0 at the threshold, so we predict that if it is used appropriately, the collisional broadening at low masses is suppressed, as resonances decay immediately after formation.

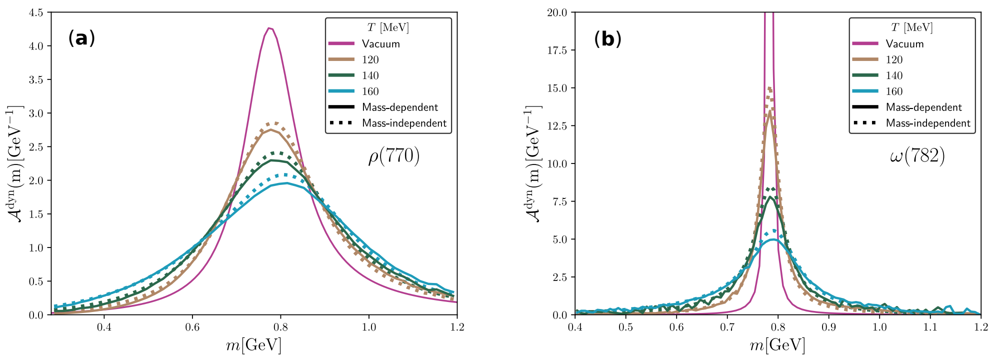

Figure 8. Dynamical spectral function of the (**a**) ρ and (**b**) ω mesons at different temperatures and baryochemical potential $\mu_B = 400$ MeV in thermal equilibrium under different vacuum decay assumptions.

4. Conclusions and Discussion

In this work, we investigate the collisional broadening of different particles by computing their effective width in the framework of a hadronic transport approach. First, we evolve a hadron gas to equilibrium at different temperatures and baryochemical potential $\mu_B = 400$ MeV, allowing us to establish the thermal behavior of such particles. The effective width shows dependence on the system temperature, where large temperatures enhance the collisional broadening of all hadron species except the $a_1(1260)$ meson, which does not have any absorption channel available. The particles that can broaden are generally more affected at lower masses, because the absorption cross-sections decrease at high masses.

Furthermore, we study the effect of collisional broadening in non-equilibrium systems created in HICs. In this framework, the effective width shows dependence on the system size, as collisional broadening is enhanced by a larger system. We observe that each resonance behaves differently, depending on when it is produced the most. $\Delta(1232)$

baryons show a behavior similar in both the thermal gas and HICs, since they are mostly created in the first NN interactions and move across a relatively thermalized medium [8]. On the other hand, $K^*(892)$ mesons, being strange particles, tend to appear after the third interactions, when the medium has already dissipated.

We also investigate the processes that cause a collisional broadening of ρ mesons. Particularly, the contribution of the $\rho N \to N(1520)$ absorption channel shows a significant effect around $m_\rho \approx 0.5$ GeV. In agreement with the full in-medium model [3,22], the coupling to nucleons is the most important, with π coupling being a distant second. We also find that the pole mass of the outgoing particle in each absorption channel determines the peaks in their contribution to collisional broadening, with some differences to account for the final kinetic energy.

Lastly, we compare two assumptions for the decay probability in vacuum in the thermal gas framework. We observe that a mass-dependent description of Γ^{dec} slightly enhances collisional broadening close to the pole mass.

Author Contributions: Conceptualization, R.H. and H.E.; Methodology, R.H.; Data curation, B.B.; Writing—original draft, B.B.; Writing—review and editing, R.H.; Supervision and Project administration, H.E. All authors have read and agreed to the published version of the manuscript.

Funding: This work was supported by Helmholtz Forschungsakademie Hessen für FAIR (HFHF). The authors also acknowledge the support by the State of Hesse within the Research Cluster ELEMENTS (Project ID 500/10.006) and by Deutsche Forschungsgemeinschaft (DFG; German Research Foundation)—Project number 315477589—TRR 211.

Data Availability Statement: The data presented in this study are openly available from FigShare at https://figshare.com/articles/dataset/Data-Balinovic_zip/23695755. Accessed on 6 September 2023.

Acknowledgments: Computational resources were provided by GreenCube at GSI.

Conflicts of Interest: The authors declare no conflicts of interest.

Appendix A. Interaction Cross-Sections

As discussed in Section 3, the collisional broadening of a particle results from the processes where it is absorbed, which are determined by inelastic cross-sections. These are functions of the center-of-mass energy between the incoming particles and thus depend on the off-shell mass of each, as well as on the relative momenta. We exemplify this in Figure A1, which shows the inelastic cross-sections for $\omega + p$ and $\omega + \pi$ scatterings and how they depend on the excess energy for different values of m_ω.

In the thermal hadron gas, the inelastic processes consist of $2 \to 1$ and $2 \to 2$ interactions. The peaks of each cross-section are always around the same $\sqrt{s}$, so the peaks in *excess* energy trivially shift with the increase in resonance mass. This happens until the peak cannot shift any further, since the center-of-mass energy is bounded from below by the sum of incoming masses. After this, heavier resonances have a progressively smaller σ_{inel}, and consequently a smaller collisional width, as seen in Figure 2a. The incoming particles still interact, but mostly through elastic scattering, which does not cause collisional broadening.

Figure A2 shows the cross-sections of $p + p$ scatterings that happen in the first moments of an HIC. For energies below $\sqrt{s} = 3.5$ GeV, the largest inelastic contribution is the excitation of Δ via $NN \to N\Delta$, followed by double Δ production. This is why the Δ baryons in the nuclear collisions of Section 3.2 behave similarly to the those in the thermal gas of Section 3.1. Other $2 \to 2$ channels are possible but very unlikely, with branching ratio $\sigma/\sigma_{\text{tot}} \leq 2\%$.

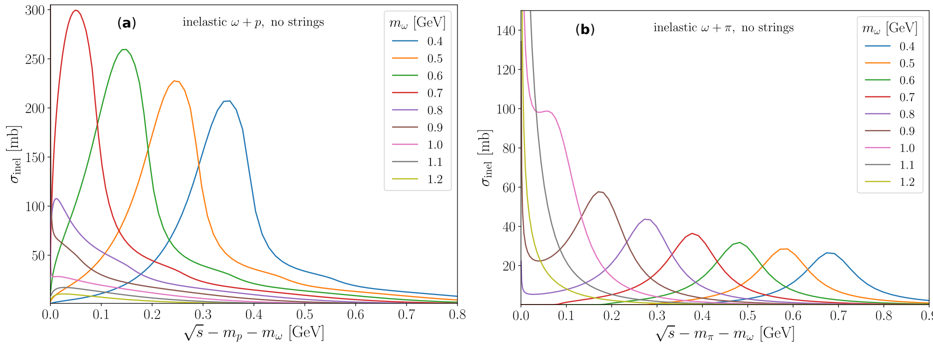

Figure A1. Inelastic cross-sections of (**a**) $\omega + p$ and (**b**) $\omega + \pi$ scatterings in a thermal gas for different off-shell masses m_ω.

Between $\sqrt{s} = 3.5$ and 4.5 GeV, we use a transition from the resonance to the string picture, with non-diffractive string fragmentations quickly dominating; above that, only strings are produced.

Concerning the $K^*(892)$ meson, the lowest mass states that can decay into it are $N(1875)$ and $\Delta(1900)$, both of which are rarely produced in these interactions. The systems analyzed in Section 3.2 have $\sqrt{s_{NN}} = 2.32$–2.41 GeV, so most $K^*(892)$ will be produced from a tertiary or later interaction.

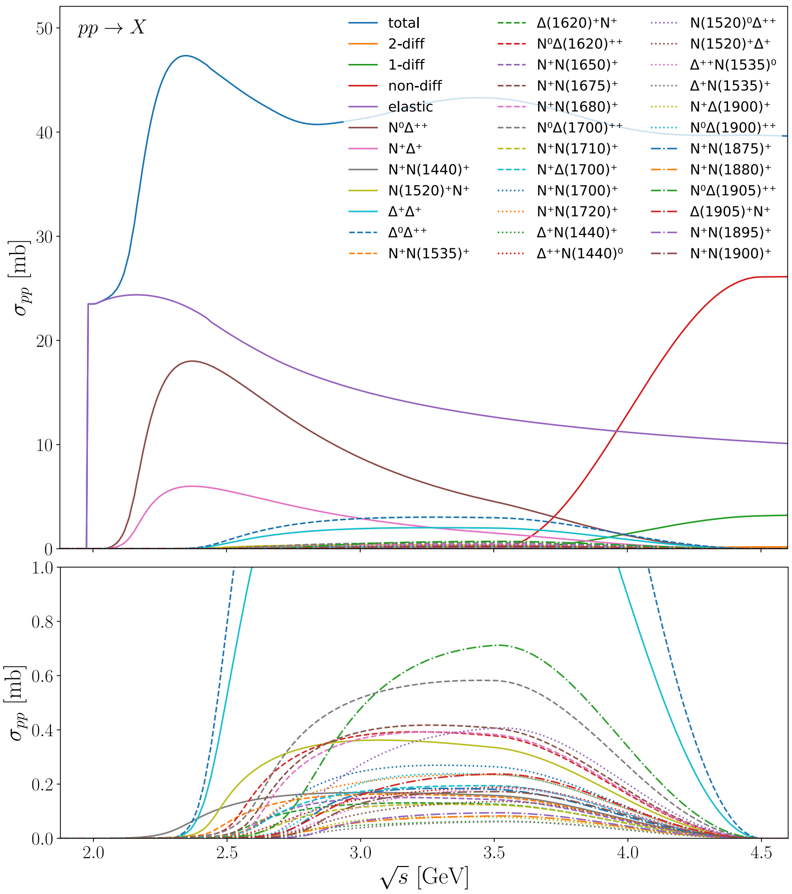

Figure A2. Cross-sections of $p + p$ scatterings we use in a nuclear collision, including string fragmentation ("2-diff", "1-diff", and "non-diff"). Below is an enlargement of smaller contributions.

Notes

1 We consider stable the hadrons with $\Gamma_0 \leq 10$ keV.

2 In collisions with energies higher than $\sqrt{s_{NN}} \approx 3.5$ GeV, strange hadrons also come from string fragmentation (see Appendix A).

[3] The difference from the actual peak is due to the kinetic energy given to the created resonance.

References

1. Larionov, A.B.; Effenberger, M.; Leupold, S.; Mosel, U. Resonance lifetime in BUU: Observable consequences. *Phys. Rev. C* **2002**, *66*, 054604. [CrossRef]
2. Rapp, R.; Wambach, J. Low mass dileptons at the CERN SPS: Evidence for chiral restoration? *Eur. Phys. J. A* **1999**, *6*, 415–420. [CrossRef]
3. van Hees, H.; Rapp, R. Dilepton Radiation at the CERN Super Proton Synchrotron. *Nucl. Phys. A* **2008**, *806*, 339–387. [CrossRef]
4. Buss, O.; Gaitanos, T.; Gallmeister, K.; van Hees, H.; Kaskulov, M.; Lalakulich, O.; Larionov, A.B.; Leitner, T.; Weil, J.; Mosel, U. Transport-theoretical Description of Nuclear Reactions. *Phys. Rept.* **2012**, *512*, 1–124. [CrossRef]
5. Linnyk, O.; Bratkovskaya, E.L.; Ozvenchuk, V.; Cassing, W.; Ko, C.M. Dilepton production in nucleus-nucleus collisions at top SPS energy within the Parton-Hadron-String Dynamics (PHSD) transport approach. *Phys. Rev. C* **2011**, *84*, 054917. [CrossRef]
6. Endres, S.; van Hees, H.; Weil, J.; Bleicher, M. Coarse-graining approach for dilepton production at energies available at the CERN Super Proton Synchrotron. *Phys. Rev. C* **2015**, *91*, 054911. [CrossRef]
7. Endres, S.; van Hees, H.; Weil, J.; Bleicher, M. Dilepton production and reaction dynamics in heavy-ion collisions at SIS energies from coarse-grained transport simulations. *Phys. Rev. C* **2015**, *92*, 014911. [CrossRef]
8. Staudenmaier, J.; Weil, J.; Steinberg, V.; Endres, S.; Petersen, H. Dilepton production and resonance properties within a new hadronic transport approach in the context of the GSI-HADES experimental data. *Phys. Rev. C* **2018**, *98*, 054908. [CrossRef]
9. Hirayama, R.; Staudenmaier, J.; Elfner, H. Effective spectral function of vector mesons via lifetime analysis. *Phys. Rev. C* **2023**, *107*, 025208. [CrossRef]
10. Weil, J.; Steinberg, V.; Staudenmaier, J.; Pang, L.G.; Oliinychenko, D.; Mohs, J.; Kretz, M.; Kehrenberg, T.; Goldschmidt, A.; Bauchle, B.; et al. Particle production and equilibrium properties within a new hadron transport approach for heavy-ion collisions. *Phys. Rev. C* **2016**, *94*, 054905. [CrossRef]
11. Olive, K.A. et al. [Particle Data Group] Review of Particle Physics. *Chin. Phys. C* **2014**, *38*, 090001. [CrossRef]
12. Manley, D.M.; Saleski, E.M. Multichannel resonance parametrization of pi N scattering amplitudes. *Phys. Rev. D* **1992**, *45*, 4002–4033. [CrossRef] [PubMed]
13. Danielewicz, P.; Pratt, S. Delays associated with elementary processes in nuclear reaction simulations. *Phys. Rev. C* **1996**, *53*, 249–266. [CrossRef]
14. Bass, S.A.; Belkacem, M.; Bleicher, M.; Brandstetter, M.; Bravina, L.; Ernst, C.; Gerland, L.; Hofmann, M.; Hofmann, S.; Konopka, J.; et al. Microscopic models for ultrarelativistic heavy ion collisions. *Prog. Part. Nucl. Phys.* **1998**, *41*, 255–369. [CrossRef]
15. Li, Q.; Bleicher, M. A Model comparison of resonance lifetime modifications, a soft equation of state and non-Gaussian effects on pi-pi correlations at FAIR/AGS energies. *J. Phys. G* **2009**, *36*, 015111. [CrossRef]
16. Schumacher, D.; Vogel, S.; Bleicher, M. Theoretical analysis of dilepton spectra in heavy ion collisions at GSI-FAIR energies. *Acta Phys. Hung. A* **2006**, *27*, 451–458. [CrossRef]
17. Reichert, T.; Bleicher, M. Kinetic mass shifts of $\rho(770)$ and $K^*(892)$ in Au+Au reactions at $E_beam = 1.23\ A$GeV. *Nucl. Phys. A* **2022**, *1028*, 122544. [CrossRef]
18. Sjöstrand, T.; Ask, S.; Christiansen, J.R.; Corke, R.; Desai, N.; Ilten, P.; Mrenna, S.; Prestel, S.; Rasmussen, C.O.; Skands, P.Z. An introduction to PYTHIA 8.2. *Comput. Phys. Commun.* **2015**, *191*, 159–177. [CrossRef]
19. Agakishiev, G. et al. [HADES Collaboration] Study of dielectron production in C+C collisions at 1-A-GeV. *Phys. Lett. B* **2008**, *663*, 43–48. [CrossRef]
20. Adamczewski-Musch, J. et al. [HADES Collaboration] Centrality determination of Au + Au collisions at 1.23A GeV with HADES. *Eur. Phys. J. A* **2018**, *54*, 85, [CrossRef]
21. Vogel, S.; Bleicher, M. Reconstructing ρ 0 and ω mesons from nonleptonic decays in C+ C collisions at 2 GeV/nucleon in transport model calculations. *Phys. Rev. C* **2006**, *74*, 014902. [CrossRef]
22. Rapp, R.; Gale, C. ρ properties in a hot meson gas. *Phys. Rev. C* **1999**, *60*, 024903. [CrossRef]